Published in final edited form as:

Acta Biomater. 2021 May ; 126: 170–182. doi:10.1016/j.actbio.2021.03.013.

Nanofibrous Hyaluronic Acid Scaffolds Delivering TGF-β3 and SDF-1α for Articular Cartilage Repair in a Large Animal Model

Anthony R. Martin, MD, MSTR[1,2], **Jay M. Patel, PhD**[1,4], **Ryan C. Locke, PhD**[1], **Michael R. Eby, MD**[2], **Kamiel S. Saleh, BSE**[1], **Matthew D. Davidson, PhD**[3], **Mackenzie L. Sennett, BS**[1], **Hannah M. Zlotnick, BSE**[1,3], **Andrew H. Chang, BA**[2], **James L. Carey, MD**[1,2], **Jason A. Burdick, PhD**[3], **Robert L. Mauck, PhD**[1,2,3,4]

[1]McKay Orthopedic Research Laboratory, University of Pennsylvania, Philadelphia, PA, 19104

[2]Perelman School of Medicine, University of Pennsylvania, Philadelphia, PA, 19104

[3]Department of Bioengineering, University of Pennsylvania, Philadelphia, PA, 19104

[4]Translational Musculoskeletal Research Center, Corporal Michael J. Crescenz Veterans Affairs Medical Center, Philadelphia, PA, 19104

Abstract

Focal cartilage injuries have poor intrinsic healing potential and often progress to osteoarthritis, a costly disease affecting almost a third of adults in the United States. To treat these patients, cartilage repair therapies often use cell-seeded scaffolds, which are limited by donor site morbidity, high costs, and poor efficacy. To address these limitations, we developed an electrospun cell-free fibrous hyaluronic acid (HA) scaffold that delivers factors specifically designed to enhance cartilage repair: Stromal Cell-Derived Factor-1α (SDF-1α; SDF) to increase the recruitment and infiltration of mesenchymal stem cells (MSCs) and Transforming Growth Factor-β3 (TGF-β3; TGF) to enhance cartilage tissue formation. Scaffolds were characterized *in vitro* and then deployed in a large animal model of full-thickness cartilage defect repair. The bioactivity of both factors was verified *in vitro*, with both SDF and TGF increasing cell migration, and TGF increasing matrix formation by MSCs. *In vivo*, however, scaffolds releasing SDF resulted in an inferior cartilage healing response (lower mechanics, lower ICRS II histology score) compared to scaffolds releasing TGF alone. These results highlight the importance of translation into large animal models to appropriately screen scaffolds and therapies, and will guide investigators towards alternative growth factor combinations.

Graphical Abstract

*Please address correspondence to Dr. Robert L. Mauck, 308A Stemmler Hall, 3450 Hamilton Walk, Philadelphia, PA, 19104-6081, lemauck@mail.med.upenn.edu, Phone: +1 215-898-8653, Fax: +1 215-573-2133.

Declaration of interests

The authors declare that they have no known competing financial interests or personal relationships that could have appeared to influence the work reported in this paper.

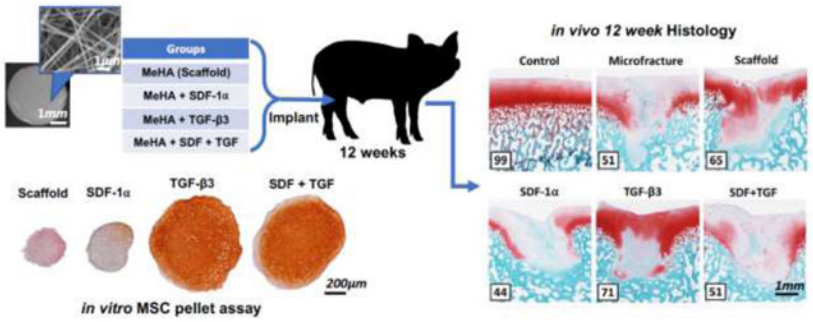

Keywords

Cartilage; hyaluronic acid; electrospinning; growth factors

1. Introduction

Articular cartilage is a remarkably durable tissue that withstands significant compressive and shear forces with daily use. However, following traumatic injury, cartilage lacks the intrinsic potential to regenerate [1]. Focal injury to cartilage, if not treated, can eventually lead to degenerative osteoarthritis [2], a debilitating ailment affecting 37% of adults in the United States [3]. Existing therapies for focal cartilage injuries have room for improvement. The traditional microfracture (MFx) technique involves penetration of the subchondral bone at the base of the defect to release marrow elements and create a blood clot that fills the defect [4]. However, this clot remodels into mechanically-inferior fibrocartilage that cannot support the loading required of larger lesions (>2cm^2) [5]. Alternatively, Matrix-Assisted Autologous Chondrocyte Implantation (MACI) has become the modern gold standard for focal cartilage defect restoration in North America and several parts of Europe [6–10]. This technique typically involves a preliminary procedure to harvest healthy non load-bearing cartilage, ex-vivo chondrocyte isolation and expansion, seeding of these chondrocytes onto a collagen or hyaluronan membrane and culture over several weeks, and a second procedure to implant the seeded collagen membrane into the cartilage defect. Although MACI has excellent results in select patient populations, it is limited by significant costs, the need for two procedures, donor site morbidity, and high failure rates in non-ideal candidates [11–13].

Augmented microfracture is another modern therapy that uses a single stage procedure to implant a cell-free biomaterial matrix into a cartilage defect after MFx has been performed [14–17]. Augmented microfracture represents a simpler, more affordable alternative to cell-culture based therapies (e.g. MACI). Without seeded cells, however, it may produce a less robust regenerate tissue than its cell-seeded counterparts. The efficacy of augmented microfracture may be strengthened with the addition of bioactive molecules to enhance cartilage repair [18]. For example, pre-clinical studies have shown that fibroblast growth factor 18 (FGF-18) delivered on a collagen membrane potentiated the healing of a MFx-treated cartilage defect in sheep [19]. Similarly, our work showed that transforming growth factor beta 3 (TGF-β3) delivered from electrospun hyaluronic acid (HA) or polycaprolactone (PCL) scaffolds improved histological metrics of MFx-treated cartilage defects in pigs [20].

TGF-β3 delivery also increased cell recruitment into osteochondral defects in rabbits [21]. A number of other growth factors have also shown promise in terms of augmenting cartilage repair *in vivo* by improving cell differentiation towards a chondrogenic phenotype, including BMP-2, BMP-7, IGF-1, and TGF-β1 [18,22].

Improvements to augmented microfracture noted above are largely focused on improving the amount of cartilage tissue deposition in the repair site. However, the efficacy of augmented microfracture may be further improved by increasing the number of cartilage precursor cells that are able to migrate to the defect site and into the implanted scaffold. A number of approaches have been proposed to address this issue, including different scaffold fabrication techniques [23,24] as well as local chemokine release [25,26]. Stromal cell-derived factor 1 alpha (SDF-1α) is a potent chemokine that can recruit endogenous stem cells into biomaterial scaffolds and allografts *in vitro*, as well as in small animal models of cartilage repair [26–29]. Few studies, however, have attempted combinatorial biofactor delivery in order to improve the migration of endogenous cells into the defect/scaffold site, and then to guide the differentiation of these cells towards a chondrogenic phenotype [30,31].

Thus, the objective of this study was to determine the effects of SDF-1α and TGF-β3, and their combination, on cartilage regeneration in a large animal model of focal cartilage defect repair. Electrospun HA was chosen as the scaffold material because of its natural presence within the cartilage extracellular matrix, its common use in therapeutic intra-articular injections, as well as its ability to enhance the chondrogenesis of MSCs derived from bone marrow [32,33]. SDF-1α and TGF-β3 were chosen for their chemotactic and chondrogenic properties, respectively, both having been previously verified separately *in vivo* [20,28,34,35]. We hypothesized that these two biofactors, when released from HA nanofibrous scaffolds, would synergistically improve cartilage regeneration. To test this hypothesis, we implanted scaffolds in a Yucatan minipig model of cartilage defect repair, and analyzed several repair outcomes at 12 weeks, including second look arthroscopy, biomechanics, subchondral remodeling, and histological scoring.

2. Methods

2.1. Material Synthesis and Characterization

HA (Lifecore Biomedical, 76kDa) was methacrylated (MeHA) as previously reported, and approximately 42% of the primary hydroxyl groups were modified [36,37]. To facilitate cell adhesion, cystine containing RGD (GCGYGRGDSPG, Genscript) peptides were conjugated to the MeHA backbone via a Michael addition reaction between the thiols on cystine and methacrylate groups on HA. Briefly, MeHA was dissolved to a final concentration of 0.2 w/v% in TEOA buffer (pH 8.0) and RGD peptides (0.3mM) were added to the solution, mixed for 30 minutes at 37 °C, reacted overnight at 37 °C, dialyzed for 10 days, and lyophilized [32]. Based on the efficiency of previous reactions, ~0.3% of the methacrylate groups were modified with RGD containing peptides.

2.2. Electrospun Scaffold Fabrication

The electrospinning solution was prepared containing the synthesized MeHA (4% w/v), polyethylene oxide (PEO, Sigma, 900kDa, 2% w/v), and Irgacure 2959 (Sigma, 0.05% w/v) in dd$H_2$0. The PEO serves to increase the solution viscosity during electrospinning to improve fiber formation, but then later dissolves out of the scaffold when it is hydrated. The Irgacure 2959 within the solution is a photoinitiator that enables the crosslinking of MeHA under ultraviolet (UV) light via free radical generation after fibers are collected.

This solution was electrospun onto a rotating mandrel using a custom apparatus [23,24,32,38]. In brief, 7 mL of solution were loaded into a 10 mL syringe fitted with a blunt 18 gauge metal needle. A positive voltage of 18 kV was applied to the needle and a negative voltage of 2 kV was applied to a metal rotating collecting mandrel. A syringe pump was used to extrude the solution at a rate of 0.4 mL/h. Metal deflectors with a positive voltage of 5 kV were used to focus the spray of fibers onto the mandrel. After the syringe was emptied, a central strip of scaffold was cut and peeled off of the mandrel. The scaffold was placed into a clear plastic bag that was purged with nitrogen gas. Finally, a UV lamp (320nm, Lumen Dynamics OmniCure S2000) was used to crosslink each side of the collected MeHA fiber mat for 30 minutes.

In this study, four scaffold groups were fabricated, using the same procedure: scaffold without biofactor (Scaffold), scaffold with SDF-1α (SDF), scaffold with TGF-β3 (TGF), and scaffold with both SDF-1α and TGF-β3 (S+T). Growth factors were added to the spinning solution at a mass of 10 μg SDF-1α (recombinant human, R&D Systems) and 50 μg TGF-β3 (recombinant human, R&D Systems). A biopsy punch was used to cut circular scaffold samples 4.5mm in diameter to obtain an estimated growth factor mass of 21.25 ng SDF-1α and 106.29 ng TGF-β3 per scaffold. This dosing was chosen based on effective concentrations seen in our previous studies and the literature, and assuming 50% release from scaffolds [20,27,34]. Scaffolds were stored in nitrogen-purged containers at −80° C for less than 3 months prior to use.

2.3. Scaffold Characterization

Scaffolds from all four groups were imaged with an environmental scanning electron microscope (SEM; FEI Quanta 600) at 40,000x magnification, and ImageJ software [39] was used to measure fiber diameter (n=10 images) (Figure 1A). Scaffold thickness was measured with a custom LVDT laser probe measurement device [40] in the dry state, as well as after hydration in PBS at 37°C for 1, 24, and 48 hours (n=4). Dissolution of the scaffold was measured by incubating scaffolds in 1% BSA in PBS on a shaker at 37°C (n=8). Aliquots of supernatant were taken at 24 hours, 1 week, 2 weeks, and 5 weeks, and the aliquot volume (100 μl of 1000 μl) was replaced with fresh solution. Aliquots were measured in duplicate for HA content using the uronic acid assay, as previously described [41]. Remaining HA content was determined by completely degrading the scaffold at the final time point with hyaluronidase (type IV, bovine testes, Sigma) (n=8). Biofactor release profiles were measured by incubating scaffolds in 1% BSA in PBS on a shaker at 37°C (n=3). The medium was completely removed and replaced at 1 hour, 1 day, 3 days, and 6 days. After the final time point, remaining biofactor within the scaffold was determined by

completely degrading the scaffolds with hyaluronidase (type IV, bovine testes, Sigma). The medium collected at each time point and final degradation was measured for biofactor content using an Enzyme-Linked Immunosorbent Assays for SDF-1α and TGF-β3 (Duoset ELISA, R&D Systems).

2.4. *In Vitro* Assessment of Scaffold Bioactivity

To address migratory activity, scaffolds were sterilized with UV light (CL-1000 UV Crosslinker, UVP) for 30 minutes on each side and seeded with bone marrow-derived juvenile bovine mesenchymal stem cells (jbMSCs) (n=5). jBMSCs were isolated from juvenile (1–3 weeks old) bovine stifle joints (Research 87, Boylston MA) by harvesting subchondral bone marrow from the femoral condyles. Marrow blocks were shaken in heparin-containing (0.2% w/v heparin) Dulbecco‟s modified Eagle‟s medium (DMEM), and the resulting solution was centrifuged, resuspended in basal media, and plated for expansion. Dry scaffolds were seeded with 500k P1 cells (1M cells/mL) in 500 mL of chemically defined media (CM-: high glucose Dulbecco‟s Modified Eagle‟s Medium with 1x penicillin/streptomycin, 0.1mM dexamethasone, 50 mg/mL ascorbate 2-phosphate, 40 mg/mL l-proline, 1mM sodium pyruvate, 1.25 mg/mL BSA) containing 1 million cells/mL in a low-adhesion 24-well plate (n=5). The plate was incubated at 37°C for 7 days with media changes on days 3 and 6. Scaffolds were then carefully removed from media, rinsed with PBS, fixed, and stained to visualize nuclei (Hoechst 33342, ThermoFisher) and F-actin (Phalloidin-Alexa Fluor 488, ThermoFisher). Scaffolds were then cut in cross-section at the largest diameter using an 11-blade scalpel. Scaffolds were placed cut-side-down on glass slides and supported on both sides with glass cover slips. A confocal microscope (Nikon A1R) was used to image cell infiltration into the center of the scaffold. Infiltration was quantified using a custom MATLAB algorithm (MathWorks) based on a fluorescence threshold and nuclei distance from the seeded scaffold surface [24,38,42]. The MATLAB program identified nuclei from Hoechst staining, calculated the centroid of nuclei, and measured the distance from this centroid to the scaffold edge (measured perpendicularly to the scaffold edge). These distances were calculated for one large ROI per scaffold (n=5 scaffolds per group).

To assess the chondrogenic bioactivity of factors released from scaffolds, we performed an assay where pellets of jMSCs were co-cultured with each of the four groups of sterile scaffolds. jbMSCs (250,000 in 250μL media) were centrifuged in 96-well V-bottom plates at 300g for 5 minutes and allowed to form pellets for 48 hours. Pellets were then co-cultured with each of the four groups of sterile scaffolds in a non-adherent (non tissue culture treated) 24-well plate with 0.5mL of CM- media changed twice weekly (n=12). Pellets and scaffolds were kept on opposing sides of the well to prevent contact and cell egress from the pellet to the scaffold, while still allowing released factors to influence the cell pellet. Positive control groups without scaffold, but with soluble biofactors were also maintained for each group. These included CM-media, CM-S media (CM- with 10ng/mL soluble SDF-1α), CM-T media (CM- with 10ng/mL soluble TGF-β3), and CM-S+T (CM- with 10ng/mL soluble SDF-1α and 10ng/mL soluble TGF-β3) (n=12). After 5 weeks of culture, pellets were digested overnight with Proteinase-K (Fisher BioReagent). Sulfated glycosaminoglycan content was measured with the 1,9-dimethylmethlene blue (DMMB) dye-binding assay and

DNA content was measured with the PicoGreen assay (Quant-iT Invitrogen) (n=4). Additional pellets were fixed in 4% paraformaldehyde (PFA), embedded in optimal cutting temperature (OCT) compound, and sectioned on a cryotome for histological evaluation with Safranin O (0.2%) and Fast Green (0.05%) staining (n=4), as well as Picrosirius red (1%) staining (n=2–4). Immunohistochemistry staining for Type II collagen (Abcam) was also performed on the pellet groups co-cultured with scaffold (n=2–4).

2.5. Large Animal Study

All scaffolds were sterilized with UV light (CL-1000 UV Crosslinker, UVP) for 30 minutes on each side. Bilateral procedures were performed on 6 castrated male juvenile Yucatan minipigs (6 months old, 30–35kg, Sinclair Bioresources) under protocols approved by the Institutional Animal Care and Use Committee (IACUC). Alendronate (40mg daily) was administered orally in a fasting state for 2 weeks prior to surgery, and over the entire duration of the study, to minimize subchondral remodeling [43–45].

2.5.1. Surgical Procedure—A minimally invasive surgical protocol under general endotracheal anesthesia (isoflurane/buprenorphine) was utilized to access the porcine trochlea [46,47]. Through a 5cm medial patellar arthrotomy, four cylindrical full-thickness chondral defects were created in the trochlea using a 4mm biopsy punch and small curette, exposing the subchondral bone plate. An awl was then used to make three microfracture (MFx) holes in each defect, each approximately 0.5mm in diameter and 1mm deep into the subchondral bone [20]. One defect per joint was left untreated (no scaffold), serving as a MFx control, and the remaining three defects were treated with scaffolds from the same group (Table 1) (n=3 animals, 3 replicates per knee, 1 MFx control per knee). This allowed for normalization to the MFx control within the same joint. Scaffold groups were isolated per joint to avoid cross defect interactions of biofactors. Scaffolds were randomized to joints and to defects within joints, with no animal receiving the same group in both knees. Scaffolds were allowed to hydrate in situ with marrow elements, followed by fixation with a combination of press-fit technique (4.5mm scaffold in 4mm defect) and fibrin sealant (TISSEEL, Baxter) prior to closure. The capsule, subcutaneous tissue, and skin were closed in layers, and the animal was recovered from anesthesia. Post-operative medications consisted of buprenorphine (0.01mg/kg intramuscular twice daily for 3 days) and cephalexin (250 mg oral daily for 3 days) [47]. Animals were euthanized 12 weeks after scaffold implantation.

2.5.2. Second Look Arthroscopy—Second-look arthroscopy was performed immediately following euthanasia, for evaluation with the International Cartilage Repair Society (ICRS) cartilage repair assessment and the Oswestry Arthroscopic Scoring system (OAS) [48]. Standardized arthroscopic photos of all defects were randomized and scored by four trained, blinded reviewers (n=3 × 3 replicates). For the OAS system, the surgeon performing the arthroscopy determined the stiffness on probing score with a right angle probe; the surgeon was blinded to treatment. All other scores were averaged among the four reviewers. The stifle joint was then opened, and the entire trochlea was photographed and harvested en bloc along with the subchondral bone. Samples were then immediately

immersed in PBS with protease inhibitors (Sigma) and stored at 4°C overnight until mechanical testing the following day.

2.5.3. Mechanical Testing—Trochleae were divided into osteochondral quadrants using a band saw to separate the four defects on each trochlea. Two additional proximal segments served as non-defected (intact) controls. Blocks were potted in polymethyl methacrylate (PMMA), immersed in PBS with protease inhibitors, and loaded into a custom Instron testing set up. Indentation testing was conducted using an Instron 5848 electromechanical system with a 2mm-diameter spherical indentation probe [49] (n=3 × 3 replicates). Briefly, the indenter was advanced perpendicular to the middle of the defect surface, and four steps of 10% strain were applied. Steps were held for 600 seconds while measuring the resultant stress relaxation. A custom MATLAB algorithm was used to extract Young‟s modulus at equilibrium after the 3rd strain step. Following mechanical testing, samples were removed from PMMA and fixed in 4% PFA for 24 hours.

2.5.4. Micro-Computed Tomography (μCT)—Fixed osteochondral samples were stained with Lugol‟s solution (Sigma-Aldrich) overnight to enable visualization of the cartilage, and were then imaged with a μCT scanner (VivaCT 40, Scanco Medical) at a voxel size of 10.5 μm, and energy of 70 kV, 85 μA. ITK-SNAP software [50] was used to segment the subchondral bone resorption volume in a semi-automated fashion (Figure 6A) (n=3 × 3 replicates). In brief, segmentation bubbles were placed in the center of the defect and allowed to expand until they encountered a bony boundary and completely filled the defect. Boundaries were defined with the classification method and the active contour evolution (region competition force = 1, smoothing force = 1). After the bony defect was completely segmented, the segmentation was manually trimmed at the cartilage boundary to be flush with the surrounding subchondral bone surface. After scans, samples were incubated in PBS for 24 hours to remove the Lugol‟s solution. Samples were then decalcified in formic acid (Formical-2000, StatLab) for 4 weeks.

2.5.5. Histological Assessment—Decalcified samples were processed for histology and embedded in paraffin wax. Microtome sections (8 μm) from the cross-section with the largest defect diameter were stained using Safranin-O (0.2%)/Fast Green (0.05%) or Alcian Blue (1%)/Picrosirius Red (0.1%), and imaged under bright field or polarized light, respectively. Three blinded independent observers scored defect and control sections using the ICRS II Histological Assessment Scale [51] (n=3 × 3 replicates) (Supplementary Table 1). Scores, ranging from 0–100% (worst-best), were averaged amongst the 3 observers. Immunohistochemistry staining for Type II collagen (Abcam ab34712) was also performed on the best, median, and worst-scoring samples from each group.

2.6. Statistical Methods

A priori power analysis (G*Power 3.1) using mean and standard deviation data from prior studies was used to calculate the minimum sample size to achieve a power of 0.9 and an alpha of 0.05. GraphPad Software (PRISM 6) was used to run all statistical tests with a $p < 0.05$ considered significant. Outliers were removed from the data set via the ROUT method with a Q=1%. Normal data were compared using ANOVA with Tukey‟s post hoc analysis,

assuming equal variance. Non-normal data were compared using the Mann-Whitney test or Kruskal-Wallis test with Dunn‟s nonparametric multiple comparisons. For the large animal model, the three replicates per joint were normalized to the MFx-only-treated defect within the same joint.

3. Results

3.1. Scaffold Fabrication and Characterization

MeHA scaffolds (+/− growth factor(s)) were electrospun and crosslinked using the same MeHA polymer and electrospinning parameters, ensuring that the structural and mechanical properties, and the degree of crosslinking were constant across treatment groups. SEM analysis (Figure 1A) of the dry scaffolds after electrospinning showed that fiber diameter was not significantly different among the four scaffold groups and averaged 190 +/− 6 nm (Figure 1B). Scaffold thickness measured 0.49 +/− 0.03 mm when dry; scaffolds swelled by roughly 3 fold to 1.45 +/− 0.09 mm after 48 hours of hydration (Figure 1C). There was no significant difference in thickness between scaffold groups at any time point (p=0.60). Scaffolds displayed similar degradation profiles (p=0.54), with roughly 50% of total HA released after 5 weeks of incubation (Figure 1D). Total HA content per scaffold averaged 0.57 +/− 0.03 mg after complete degradation with hyaluronidase (Scaffold 0.54 mg, SDF 0.59 mg, TGF 0.56 mg, S+T 0.61 mg). ELISA assay revealed that SDF and S+T scaffolds released 28 +/− 5% and 68 +/− 3%, respectively, of total SDF-1α released at 1 hour (Figure 1E). At 1 day, release reached levels of 56 +/− 9% and 76 +/− 3% of total SDF-1α release for the S and S+T groups, respectively. At 6 days, release was similar at 86 +/− 4% and 91 +/− 1% of total SDF-1α released. A maximum release of 7.8 +/− 0.4ng of SDF-1α was measured for the SDF group, and a maximum release of 8.1 +/− 0.5ng of SDF-1α was measured for the S+T group. ELISA for TGF-β3 revealed that TGF and S+T scaffolds released 67 +/− 6% and 79 +/− 6%, respectively, of total TGF-β3 at 1 hour (Figure 1E). At 1 day, release reached 91 +/− 4% and 92 +/− 2% of total TGF-β3 for the TGF and S+T scaffolds, respectively. At 6 days, release was near total at 98 +/− 0% and 97 +/− 1% of total TGF-β3 released. A maximum release of 46 +/− 3ng of TGF-β3 was measured for the TGF group, and a maximum release of 50 +/− 1ng of TGF-β3 was measured for the S+T group.

3.2. *In Vitro* Scaffold Bioactivity

Cell infiltration was assessed by seeding MSCs onto scaffolds and measuring the depth of cell penetration (Figure 2A). Growth factor delivery noticeably increased cellular infiltration in SDF, TGF, and S+T groups (Figure 2B). The greatest increase was from 77 +/− 20 μm in the Scaffold group to 269 +/− 90 μm in the TGF group (Figure 2C). While all three biofactor groups trended towards having higher infiltration than the scaffold-only group, the only significant difference detected was between the Scaffold and TGF groups (p=0.014).

To assess the chondrogenic activity of scaffolds, MSC pellets were cultured with either soluble-delivered or scaffold-delivered biofactors. Scaffold delivery and soluble delivery of factors showed similar results. Both groups with TGF-β3 (TGF, S+T) trended towards increased GAG (Figure 3A) and DNA (Figure 3B) content compared to groups without TGF-β3 (Media, Scaffold, SDF). Pellets co-cultured with S+T scaffold produced

significantly more GAG than pellets co-cultured with SDF or factor-free scaffolds ($p<0.05$). Evaluation of GAG to DNA ratio showed high variability due to the low DNA content in the Scaffold and SDF groups; there was no significant difference detected between groups (Supplementary Figure 1). Histological evaluation of pellets supported the biochemical results. Pellets treated with soluble or scaffold-delivered TGF-β3 both appeared larger and stained more intensely (red) for proteoglycans (Figure 3C). All pellet groups co-cultured with scaffold in chondrogenic media demonstrated staining for type II collagen (Supplementary Figure 2). Overall, TGF-β3 trended towards inducing more cell infiltration, proliferation, and chondrogenesis compared to SDF-1α.

3.3. Scaffold Evaluation in a Large Animal Cartilage Defect Model

To assess the bioactivity of released SDF-1α and TGF-β3 in an *in vivo* setting, scaffolds were implanted into full-thickness porcine cartilage defects treated with microfracture, as previously described. All animals tolerated surgery well and were standing within 1 hour post-operatively. No differences were observed between animals with regards to weight bearing and recovery, consistent with previous studies in juvenile Yucatan minipigs. Animals continued to receive daily alendronate treatment until euthanasia at 12 weeks post-surgery, at which time their weights ranged from 40.5 to 48.0 kg (average 44.0 kg, 35% increase).

3.3.1. Arthroscopic Observations—Arthroscopy at the time of sacrifice revealed that the repair tissue varied considerably from defect to defect and joint to joint (Figure 4A, Supplementary Figure 3). Gross scoring of the defects by arthroscopy did not reveal any significant differences among the scaffold or MFx groups when comparing the raw values from either the ICRS or OAS systems. After normalizing scores to MFx controls within the same joint, however, ICRS assessment showed that the SDF group scored significantly worse than the Scaffold ($p=0.038$), TGF ($p=0.001$), and S+T ($p=0.009$) groups (Figure 4B). Similarly, the normalized Oswestry scores showed that the SDF group scored significantly worse than the Scaffold ($p=0.009$) and TGF ($p=0.009$) groups (Figure 4C). The OAS system resulted in greater variability among the scores, likely due to the incorporation of the "stiffness on probing score", which could only be assessed by the surgeon performing the arthroscopy.

3.3.2. Mechanical Testing—Mechanical evaluation was carried out at the defect site (center) and in the adjacent normal cartilage. This indentation testing showed high variability both within and between joints. Control, healthy cartilage had a mean equilibrium modulus of 1840 +/− 700 kPa, similar to values previously reported in this model [20,34]. All experimental groups had moduli that were considerably lower than native control tissue ($p<0.0041$) (Figure 5A). When comparing the MFx and four scaffold groups, the TGF group trended ($p = 0.056$) towards the highest modulus (Figure 5B). After normalizing to MFx controls, the TGF group again trended towards having the highest modulus (Figure 5C), and provided a nearly 100kPa increase in average modulus relative to the Scaffold group. Cartilage from one animal in the TGF group formed repair tissue with an average equilibrium modulus of 463 +/− 200 kPa, ~1/4 that of native control tissue.

3.3.3. Micro-Computed Tomography—MicroCT imaging was performed to assess remodeling of the subchondral bone. Despite treatment with alendronate, all defects showed considerable subchondral remodeling on μCT, regardless of treatment group. Trabecular thickness was generally increased around the defect boundary (Figure 6A). Volumetric analysis of subchondral remodeling (Figure 6B) demonstrated increased resorption in the Scaffold ($p<0.05$) and S+T ($p<0.01$) groups compared to MFx.

3.4.4. Histological Assessment—Cartilage repair was assessed by histological staining and semi-quantitative evaluation. Defects stained with Safranin O and Fast Green showed varying levels of repair quality within each group (Figure 7A). ICRS II visual histological assessment scores indicated that the TGF group trended towards having the highest score among the experimental groups; increased proteoglycan deposition was also observed in the TGF group. In terms of raw scores, native tissue had the highest values ($<0.0001<p\leq0.0268$), while the SDF group scored significantly worse than both the Scaffold ($p=0.047$) and TGF ($p=0.019$) groups (Figure 7B). Normalizing scores to MFx defects from the same knee revealed that the TGF group again significantly outscored the SDF group ($p=0.004$) (Figure 7C).

Further analysis of these histological sections using polarized light imaging demonstrated increased fibrous tissue deposition (brighter areas) in the MFx, SDF, and S+T groups (Figure 8), suggesting abnormal cartilage repair tissue formation. The Scaffold and TGF groups showed less birefringence and stained more uniformly with Alcian Blue. Immunohistochemical staining for Type II collagen demonstrated subjectively higher quality cartilage regeneration in the best-scoring Scaffold and TGF groups (Figure 9). In contrast, the SDF and S+T groups showed decreased central defect staining compared to neighboring healthy cartilage.

4. Discussion

Advances in scaffold technology for articular cartilage regeneration have grown considerably [18,22]. New scaffold materials and biofactors are continually being developed and combined to improve cartilage repair and regeneration. However, most studies evaluate these new technologies *in vitro*, but rarely translate these into clinically-relevant large animal models of cartilage repair. With the absence of such evaluation, it is difficult to judge whether promising *in vitro* findings will be operative in an *in vivo* setting. In this study, we evaluated a cell-free scaffold with dual biofactor release with the goal of augmenting cartilage repair. These scaffolds are designed to support the next generation of augmented microfracture treatments, and to be widely applicable, low cost, and deployable in an off-the-shelf manner compared to current cell-culture based treatments, such as MACI. Based on our previous work showing an effect of the *in vivo* release of TGF- β3 [20], as well as promising *in vitro* data from the field [26,28,29,35,52], our initial hypothesis was that SDF-1α release from HA-based scaffolds would improve cellular recruitment to the wound site, that this would synergize with concomitant release of TGF-β3, and that this would ultimately improving chondral repair. Contrary to this initial hypothesis, the opposite finding was observed in this study. The inclusion of SDF-1α into factor-free scaffolds and TGF-β3-containing scaffolds (Scaffold-only to SDF; TGF to S+T) led to appreciable decreases in

many of our cartilage repair metrics, and improvements in none. Since the chondrogenic capacity of the dual-growth factor scaffolds appeared greater than SDF-1α-releasing scaffolds alone, but less than TGF-β3-releasing scaffolds, it may be possible that SDF-1α reduces the positive effects that TGF-β3 provides (or that TGF-β3 partially rescues the inhibitory effects of SDF-1α).

In terms of scaffold fabrication, MeHA electrospinning resulted in similar metrics across all four scaffold groups. As expected, based on prior studies, only 40–50% of the total loaded biofactor was released by the scaffolds. A majority of this loss likely occurred during the scaffold fabrication process, particularly during the spinning solution preparation, syringe loading, and electrospinning. Once the scaffold had been collected, sterilized, sealed in nitrogen, and stored at −80°C, there was likely minimal biofactor loss. Additionally, the amount of SDF-1α and TGF-β3 released per scaffold sample was comparable to effective doses seen in the literature and our previous work [20,27,29,34,53]. The TGF-β3 appeared to release faster than the SDF-1α, about 90% release at 1 day versus 6 days, respectively. Further studies on the interactions between the biofactor molecules and the nanofibers should be conducted to explore the mechanism underlying these differences. SDF-1α released from the SDF group appeared to release slower than that released from the S+T group. Perhaps the addition of both biofactors to the same scaffold changed the initial burst release kinetics. It is unclear if this difference affected the cell culture or *in vivo* outcomes. Both the SDF and S+T groups reached about 90% release of SDF-1α at 6 days. It is not clear how these in vitro measures of release relate to that which would be seen in the Yucatan minipig cartilage defect model. Synovial fluid samples at 1 day and 6 days post-operatively could help elucidate *in vivo* release. Future translational studies could scale up scaffold fabrication to assess how electrospinning larger, thicker scaffold sheets may affect scaffold characteristics, biofactor stability, and their consistency across fabrication batches.

The bioactivity of both released biofactors was validated using *in vitro* assays. These results support the reliability of electrospun MeHA as a delivery vehicle for cartilage repair applications [20,32]. Furthermore, the literature supports the cytocompatibility of MeHA hydrogels and nanofibrous scaffolds [33,54–57]. In our *in vitro* studies, both factors performed as expected when released from the scaffold in cell culture. MSC pellet cultures demonstrated that both groups releasing TGF-β3 resulted in enhanced chondrogenesis and cell proliferation, consistent with prior studies [20,53]. Evaluation of pellet GAG/DNA showed high variability and no significant difference between groups, given the very low DNA content detected in the Scaffold and SDF groups. The MSC infiltration assay demonstrated increased cell penetration into scaffolds in the SDF, TGF, and S+T groups. While TGF-β3 is known to increase cell motility, SDF-1α was expected to have a more robust response on MSC infiltration [52,58]. This discrepancy may be explained by the markedly decreased expression of CXCR4 receptor (for SDF-1α) in MSCs expanded *in vitro* [59,60].

Future *in vitro* studies could use ELISA assays to measure the amount of biofactor in culture media at different time points. This could help elucidate if there is any sustained chondrogenic or migratory effect in the scaffold after most of the biofactors have been released and replaced with fresh media. For example, if there were to be sustained biofactor

release for only 3 days measured by ELISA, but cell infiltration or chondrogenesis continued beyond 3 days, it would suggest that a short exposure to biofactor is enough to affect longer cell-level changes. Conversely, loss of growth factor bioactivity may have also occurred. Additional in vitro studies may be required to better explore the mechanism and interplay between factors, potentially at multiple doses and time points, and to also evaluate the impact of potentially recruited inflammatory cells. Furthermore, while the bioactivity of the released factors was verified, the direct chondrogenic activity of cells seeded into the scaffold could be further explored. Finally, we recognize that the in vitro assays were performed with bovine MSC**s, which may exhibit a different behavior compared to the porcine MSCs in our animal model, as well as the other marrow and synovial-derived cell types that may fill the defect site.

Several animal models of partial and full-thickness cartilage defects, as well as osteochondral defects, have been developed in an array of animals, each with their own strengths and weaknesses [61]. Small animal models, like those in rodents and rabbits, make it easier to conduct high powered studies, and also can take advantage of transgenic or immunodeficient mice [62,63]. However, the high intrinsic healing capacity, thin cartilage, and limited joint surface area in these small animals makes translation into human subjects less direct [61]. Large animal models, such as equine models, provide the greatest similarities to humans in terms of joint size, joint angle, cartilage thickness, and healing pattern [61,64]. Indeed, cartilage repair techniques have been extensively developed in horses due to the racing industry [65]. However, experimental equine models are limited by high costs, logistical difficulties, and ethical concerns [61,66]. Minipigs represent an alternative large animal model as they provide a happy medium between rodent and equine models. Their joint size and cartilage thickness (~1.5mm) allow clinically relevant chondral lesions to be created [60]. They also accommodate open and arthroscopic surgical procedures, including second look arthroscopy, a procedure commonly used in humans to evaluate the success of a prior cartilage repair procedure [48]. Both ICRS and Oswestry arthroscopic scoring used in this study highlighted similar patterns in tissue formation, further validating their use in gross evaluation of cartilage repair.

Adult minipigs generally grow to adult human weight (~70kg), providing realistic in vivo loading on repair constructs. In addition, the physiological and repair characteristics of minipigs are similar to that of humans [67,68]. Adult minipigs (18–22 months old) have low intrinsic healing potential [69]. In the Yucatan minipig in particular, 4mm full-thickness chondral defects in the trochlear groove heal with fibrocartilage, a tissue with inferior mechanical properties compared to both normal cartilage and defects treated with tissue-engineered constructs [20,70], similar to the healing response in human defects >2cm^2. Other minipig species, like the Göttingen minipig, have also shown promise in cartilage and osteochondral repair models with similar healing and bone remodeling responses seen across minipig species [68,71]. Although juvenile minipigs (6–7 months old, 30–35kg) have a higher intrinsic healing capacity than adults [72,73], cartilage repair studies using juveniles still show measurable difference between nontreated and treated chondral lesions [20,34,74]. Juveniles have the benefits of thicker cartilage (~2mm) comparable to that of humans (2.35mm) [64], easier handling, and tolerating bilateral stifle joint surgery well.

One limitation of the large animal model used is the variation in baseline repair potential and proteoglycan content between animals. In both the Safranin O/Fast Green and the Alcian Blue/Picrosirius Red stained sections, we noted that the normal cartilage background staining varied considerably from animal to animal, but was similar between different knees in the same animal. For example, the best scoring Scaffold and TGF defects were in the same animal, and the worst scoring TGF, SDF, and MFx defects were in the same animal. The histological scoring was likely skewed by this inter-animal variability, where “good healers” and animals with more baseline proteoglycan content scored higher. This issue could be addressed by increasing the power of the study.

The largest limitation of the juvenile minipig model seen in this study was the considerable amount of subchondral bone remodeling after full-thickness chondral defect creation. To mitigate this remodeling, bisphosphonates, such as risedronate [44] and alendronate [43,45], can be used under fasting conditions to inhibit the action of osteoclasts [75]. These drugs are commonly used in humans to treat osteoporosis and have not shown any negative effects on cartilage regeneration *in vitro* or *in vivo*. It is important to avoid food around the time of bisphosphonate administration, as calcium, magnesium, and other common food elements may sequester the drug in the GI tract and prevent absorption [76]. Despite continuous alendronate treatment under fasting conditions, all defects in this study showed considerable subchondral resorption at 12 weeks. Notably, the MFx group had significantly less resorption than the Scaffold and S+T groups, suggesting that the presence of a biomaterial may have altered the trajectory of the normal healing response. This response is more pronounced with stiffer, slow-degrading materials like poly(ε-caprolactone) (PCL) [20], but was not significantly attenuated with the softer, degradable HA fiber scaffolds used here. Such substantial subchondral remodeling likely impacted other downstream outcomes of repair, including histological and mechanical assessments. One possible explanation for this phenomenon is the natural thinning of articular cartilage as the calcified cartilage tidemark progresses towards the articular surface during maturation (~1.7 mm at 6 months, ~1 mm at 9 months, when this study concluded) [68,74]. The disruption of the tide mark in juvenile minipigs (when creating full-thickness chondral defects with MFx), as well as scaffold implantation, could impede this natural calcification phenomenon at the site of the defect. Future studies could evaluate these scaffolds in skeletally mature animals, where the cartilage maturation process is complete. In addition, smaller size awls could be used for microfracture to reduce the amount of subchondral bone compaction below the cartilage defect.

In terms of the effects of SDF-1α and TGF-β3 on cartilage repair, it is clear across all metrics that SDF-1α inhibited cartilage regeneration *in vivo*, while TGF-β3 trended towards augmenting cartilage regeneration. Contrary to our initial hypothesis, we did not see a synergistic effect of dual biofactor release in the S+T group. Macroscopic repair quantified via arthroscopic imaging showed that all defects treated with SDF-releasing scaffolds scored worse than MFx controls (negative value) in both the ICRS and OAS systems. In contrast, 6 of 9 defects treated with a TGF scaffold scored better than MFx (positive value) in both systems. Similarly, histological scoring showed that 7 of 9 defects treated with an SDF scaffold scored worse than MFx controls, while 8 of 9 defects treated with a TGF scaffold scored better than MFx controls. Indentation testing also showed that the SDF group trended

towards having the lowest modulus, while the TGF group trended towards having the highest value. Interestingly, in all metrics tested, the S+T group performed somewhere in between the SDF and TGF groups, suggesting some rescue effect of TGF-β3 when both biofactors were present.

The negative effects of SDF-1α seen in this porcine model are contrary to the positive results seen in other explant and small animal studies using immune incompetent rodents or rabbits [27–29,52]. One potential explanation for this response may relate to the increased recruitment of cells other than MSCs expressing the CXCR4 surface receptor; because this receptor is also present on the hematopoetic stem cell lineage [77]. It is possible that inflammatory cells, including lymphocytes and macrophages [78], were recruited into the defect, where they may disrupt the cartilage tissue regeneration that was partially observed in the Scaffold and TGF groups. The TGF-β3 in the S+T group may partially rescue this disruption, as noted by the improvement in outcomes from the SDF group to the S+T group. The treatment of 3 cartilage defects in the same knee with SDF-1α-containing scaffold may have also amplified the local inflammatory environment in the joint. Indeed, our histological assessment using polarized light demonstrated subjectively increased fibrous tissue in the MFx, SDF, and S+T groups. Future studies could perform IHC staining for macrophages and osteoclasts to help identify cells responsible for fibrosis and bone resorption.

Another limitation of the results of this study is that they were underpowered. This can help explain why the TGF group did not significantly out-perform the Scaffold without biofactor group, although all metrics trended towards better cartilage repair with TGF-β3, as seen in prior studies [20,34,53]. Furthermore, juvenile animals were utilized due to our prior use of the animals and ability to perform procedures bilaterally (and thus increase our number of defects). In addition, longer time points in the animal model may have provided a further analysis of functional repair. Future studies could carry cartilage repair constructs out to 1 year in vivo. Despite the lack of significance seen in this study, TGF-β3 trended towards improving cartilage regeneration, supporting continued investigation of its use in cartilage repair applications.

Future studies will consider the use of alternative biofactors in combination with TGF-β3, such as FGF-18 [79] and BMP-7 [30], and will consider the use of alternative scaffold types, concentrations, and mechanics. In particular, the use of anti-inflammatory bioactive factors may also combat inhibitory effects of inflammation on in vivo cartilage formation. Better control of biofactor release from MeHA scaffolds could prioritize longer release profiles (weeks to months) [22], which would expose cells in both the acute and subacute inflammatory cascade to released biofactors. Sequential and triggered release of combinatorial biofactors could also be explored [42,80,81]. Future studies using adult Yucatan minipigs may also reduce subchondral bone remodeling after full-thickness chondral defect creation [74]. Adult minipigs also mirror humans more closely in terms of weight and reduced intrinsic healing capacity, which may increase the effect size of MeHA scaffolds compared to MFx. Lastly, increasing the defect size (>2 cm^2) would more closely mimic lesions that are indicated for treatment in humans, and may also increase the effect size of scaffolds relative to MFx alone.

6. Conclusions

The results of this study illustrate the many challenges associated with translating therapeutics from the lab bench to the clinic. We demonstrated that dual-factor release (SDF-1α and TGF-β3) from nanofibrous HA scaffolds could improve cell recruitment and matrix deposition by mesenchymal progenitor cells. Translation into a large animal cartilage repair model showed, however, that while SDF-1α has predictable effects *in vitro*, its local release in cartilage defects inhibits neo-cartilage tissue regeneration. While the mechanism underlying this negative finding is not fully elucidated, this work does demonstrate the requirement for validation of promising *in vitro* findings in an orthotopic *in vivo* setting. Further, our data here did suggest improved cartilage regeneration in defects treated with scaffolds releasing TGF-β3. This factor, in combination with MFx and other agents, should be further assessed in larger and more demanding cartilage repair studies.

Supplementary Material

Refer to Web version on PubMed Central for supplementary material.

Acknowledgements

Research reported in this publication was supported by the University of Pennsylvania and the National Center for Advancing Translational Sciences of the National Institutes of Health under award number TL1TR001880. Additional support was provided by grants from the American Orthopaedic Society for Sports Medicine, the National Institutes of Health (R01 AR056624), and the Department of Veterans Affairs (IK6 RX003416 and IK1 RX003208). The content is solely the responsibility of the authors and does not represent the official views of the National Institutes of Health or other funding agencies. The authors would also like to acknowledge Sonia Bansal, Liane Miller, Brendan Stoeckl, and Claudia Loebel for their help in conducting this research.

Abbreviations:

AMIC	autologous matrix-induced chondrogenesis
CM-	chemically defined medium
FGF-18	fibroblast growth factor 18
HA	hyaluronic acid
IACUC	institutional animal care and use committee
jbMSC	juvenile bovine mesenchymal stem cell
MACI	matrix-assisted autologous chondrocyte implantation
MeHA	methacrylated hyaluronic acid
MFx	microfracture
MSC	mesenchymal stem cells
OCT	optimal cutting temperature
PCL	poly(e-caprolactone)

SDF-1α	stromal cell-derived factor-1α
TGF-β3	transforming growth factor-β3

7. References

[1]. Buckwalter JA, Articular cartilage injuries., Clin. Orthop. Relat. Res (2002) 21–37. http://www.ncbi.nlm.nih.gov/pubmed/12218470 (accessed July 31, 2017). [PubMed: 12218470]

[2]. Smith GD, Knutsen G, Richardson JB, of P Orthopaedics Robert Jones, A clinical review of cartilage repair techniques, J Bone Jt. Surg [Br] 87 (2005) 445–9. doi:10.1302/0301-620X.87B4.

[3]. Jafarzadeh SR, Felson DT, Updated Estimates Suggest a Much Higher Prevalence of Arthritis in United States Adults Than Previous Ones, Arthritis Rheumatol 70 (2018) 185–192. doi:10.1002/art.40355. [PubMed: 29178176]

[4]. Gomoll A, Microfracture and Augments, J. Knee Surg 25 (2012) 009–016. doi:10.1055/s-0031-1299654.

[5]. Carey JL, Fibrocartilage Following Microfracture Is Not as Robust as Native Articular Cartilage, J. Bone Jt. Surgery-American Vol. 94 (2012) e80–1–2. doi:10.2106/JBJS.L.00319.

[6]. Basad E, Ishaque B, Bachmann G, Stü H, @bullet Steinmeyer Jü R., Matrix-induced autologous chondrocyte implantation versus microfracture in the treatment of cartilage defects of the knee: a 2-year randomised study, Knee Surgery, Sport. Traumatol. Arthrosc (2010). doi:10.1007/s00167-009-1028-1.

[7]. Wylie JD, Hartley MK, Kapron AL, Aoki SK, Maak TG, What Is the Effect of Matrices on Cartilage Repair? A Systematic Review, Clin. Orthop. Relat. Res 473 (2015) 1673–1682. doi:10.1007/s11999-015-4141-0. [PubMed: 25604876]

[8]. Zeifang F, Oberle D, Nierhoff C, Richter W, Moradi B, Schmitt H, Autologous Chondrocyte Implantation Using the Original Periosteum-Cover Technique versus Matrix-Associated Autologous Chondrocyte Implantation, Am. J. Sports Med 38 (2010) 924–933. doi:10.1177/0363546509351499. [PubMed: 19966102]

[9]. Saris D, Price A, Drogset JO, Podskubka A, Tsuchida A, Bezuidenhoudt M, Kili S, Levine DW, Brittberg M, SUMMIT Prospective, Randomized, Controlled Trial: Response Rates To Matrix-induced Autologous Chondrocyte Implant (MACI) Versus Microfracture (MFX) By Lesion Characteristics, Orthop. J. Sport. Med (2013). doi:10.1177/232596711 3S00029.

[10]. Saris D, Md Y, Price A, Widuchowski W, || Md, Bertrand-Marchand M, Caron J, Drogset JO, Emans P, Md Y, Podskubka A, Md Z, Tsuchida A, Kili S, Levine D, Brittberg M, {{ Md, Matrix-Applied Characterized Autologous Cultured Chondrocytes Versus Microfracture Two-Year Follow-up of a Prospective Randomized Trial, (2014). doi:10.1177/0363546514528093.

[11]. Schrock JB, Kraeutler MJ, Houck DA, McQueen MB, McCarty EC, A Cost-Effectiveness Analysis of Surgical Treatment Modalities for Chondral Lesions of the Knee: Microfracture, Osteochondral Autograft Transplantation, and Autologous Chondrocyte Implantation., Orthop. J. Sport. Med 5 (2017) 2325967117704634. doi:10.1177/2325967117704634.

[12]. Frøseth Aae T, Randsborg P-H, Lurås H, Årøen A, · Øystein, Lian B, Aae TF, Microfracture is more cost-effective than autologous chondrocyte implantation: a review of level 1 and level 2 studies with 5 year follow-up, Knee Surgery, Sport. Traumatol. Arthrosc (2018). doi:10.1007/s00167-017-4802-5.

[13]. Wylie JD, Hartley MK, Kapron AL, Aoki SK, Maak TG, Failures and Reoperations After Matrix-Assisted Cartilage Repair of the Knee: A Systematic Review, Arthroscopy 32 (2016) 386–392. doi:10.1016/j.arthro.2015.07.025. [PubMed: 26422710]

[14]. Benthien JP, Behrens P, The treatment of chondral and osteochondral defects of the knee with autologous matrix-induced chondrogenesis (AMIC): Method description and recent developments, Knee Surgery, Sport. Traumatol. Arthrosc 19 (2011) 1316–1319. doi:10.1007/s00167-010-1356-1.

[15]. Gille J, Schuseil E, Wimmer J, Gellissen J, Schulz AP, Behrens P, Mid-term results of Autologous Matrix-Induced Chondrogenesis for treatment of focal cartilage defects in the knee, Knee Surgery, Sport. Traumatol. Arthrosc (2010). doi:10.1007/s00167-010-1042-3.

[16]. Gille J, Behrens P, Volpi P, De Girolamo L, Reiss E, Zoch W, Anders S, Outcome of Autologous Matrix Induced Chondrogenesis (AMIC) in cartilage knee surgery: Data of the AMIC Registry, Arch. Orthop. Trauma Surg 133 (2013) 87–93. doi:10.1007/s00402-012-1621-5. [PubMed: 23070222]

[17]. Volz M, Schaumburger J, Frick H, Grifka J, Anders S, A randomized controlled trial demonstrating sustained benefit of Autologous Matrix-Induced Chondrogenesis over microfracture at five years, Int. Orthop 41 (2017) 797–804. doi:10.1007/s00264-016-3391-0. [PubMed: 28108777]

[18]. Martín AR, Patel JM, Zlotnick HM, Carey JL, Mauck RL, Emerging therapies for cartilage regeneration in currently excluded „red knee" populations, Npj Regen. Med 4 (2019) 12. doi:10.1038/s41536-019-0074-7. [PubMed: 31231546]

[19]. Howard D, Wardale J, Guehring H, Henson F, Delivering rhFGF-18 via a bilayer collagen membrane to enhance microfracture treatment of chondral defects in a large animal model, J. Orthop. Res 33 (2015) 1120–1127. doi:10.1002/jor.22882. [PubMed: 25721940]

[20]. Kim IL, Pfeifer CG, Fisher MB, Saxena V, Meloni GR, Kwon MY, Kim M, Steinberg DR, Mauck RL, Burdick JA, Fibrous Scaffolds with Varied Fiber Chemistry and Growth Factor Delivery Promote Repair in a Porcine Cartilage Defect Model, Tissue Eng. Part A 21 (2015) 2680–2690. doi:10.1089/ten.tea.2015.0150. [PubMed: 26401910]

[21]. Lee CH, Cook JL, Mendelson A, Moioli EK, Yao H, Mao JJ, Regeneration of the articular surface of the rabbit synovial joint by cell homing: a proof of concept study, Lancet 376 (2010) 440–448. doi:10.1016/S0140-6736(10)60668-X. [PubMed: 20692530]

[22]. Patel JM, Saleh KS, Burdick JA, Mauck RL, Bioactive Factors for Cartilage Repair and Regeneration: Improving Delivery, Retention, and Activity, Acta Biomater (2019). doi:10.1016/j.actbio.2019.01.061.

[23]. Baker BM, Gee AO, Metter RB, Nathan AS, Marklein RA, Burdick JA, Mauck RL, The potential to improve cell infiltration in composite fiber-aligned electrospun scaffolds by the selective removal of sacrificial fibers, Biomaterials (2008). doi:10.1016/j.biomaterials.2008.01.032.

[24]. Shah RP, Esterhai JL, Mauck RL, Silverstein AM, Burdick JA, Baker BM, Sacrificial nanofibrous composites provide instruction without impediment and enable functional tissue formation, Proc. Natl. Acad. Sci 109 (2012) 14176–14181. doi:10.1073/pnas.1206962109. [PubMed: 22872864]

[25]. Re"em T, Witte F, Willbold E, Ruvinov E, Cohen S, Simultaneous regeneration of articular cartilage and subchondral bone induced by spatially presented TGF-beta and BMP-4 in a bilayer affinity binding system, Acta Biomater 8 (2012) 3283–3293. doi:10.1016/J.ACTBIO.2012.05.014. [PubMed: 22617742]

[26]. Zhang W, Chen J, Tao J, Jiang Y, Hu C, Huang L, Ji J, Ouyang HW, The use of type 1 collagen scaffold containing stromal cell-derived factor-1 to create a matrix environment conducive to partial-thickness cartilage defects repair, Biomaterials 34 (2013) 713–723. doi:10.1016/j.biomaterials.2012.10.027. [PubMed: 23107295]

[27]. Yu Y, Brouillette MJ, Seol D, Zheng H, Buckwalter JA, Martin JA, Use of recombinant human stromal cell-derived factor 1α-loaded fibrin/hyaluronic acid hydrogel networks to achieve functional repair of full-thickness bovine articular cartilage via homing of chondrogenic progenitor cells, Arthritis Rheumatol 67 (2015) 1274–1285. doi:10.1002/art.39049. [PubMed: 25623441]

[28]. Zhang F, Leong W, Su K, Fang Y, Wang D-A, A Transduced Living Hyaline Cartilage Graft Releasing Transgenic Stromal Cell-Derived Factor-1 Inducing Endogenous Stem Cell Homing *In Vivo*, Tissue Eng. Part A 19 (2013) 1091–1099. doi:10.1089/ten.tea.2012.0441. [PubMed: 23167782]

[29]. Sukegawa A, Iwasaki N, Kasahara Y, Onodera T, Igarashi T, Minami A, Repair of Rabbit Osteochondral Defects by an Acellular Technique with an Ultrapurified Alginate Gel Containing Stromal Cell-Derived Factor-1, Tissue Eng. Part A 18 (2012) 934–945. doi:10.1089/ten.tea.2011.0380. [PubMed: 22097896]

[30]. Crecente-Campo J, Borrajo E, Vidal A, Garcia-Fuentes M, New scaffolds encapsulating TGF-β3/BMP-7 combinations driving strong chondrogenic differentiation, Eur. J. Pharm. Biopharm 114 (2017) 69–78. doi:10.1016/j.ejpb.2016.12.021. [PubMed: 28087378]

[31]. Cheng Z, Landish B, Chi Z, Nannan C, Jingyu D, Sen L, Xiangjin L, 3D printing hydrogel with graphene oxide is functional in cartilage protection by influencing the signal pathway of Rank/Rankl/OPG, Mater. Sci. Eng. C 82 (2018) 244–252. doi:10.1016/J.MSEC.2017.08.069.

[32]. Kim IL, Khetan S, Baker BM, Chen CS, Burdick JA, Fibrous hyaluronic acid hydrogels that direct MSC chondrogenesis through mechanical and adhesive cues, Biomaterials 34 (2013) 5571–5580. doi:10.1016/j.biomaterials.2013.04.004. [PubMed: 23623322]

[33]. Chung C, Burdick JA, Influence of Three-Dimensional Hyaluronic Acid Microenvironments on Mesenchymal Stem Cell Chondrogenesis, Tissue Eng. Part A 15 (2009) 243–254. doi:10.1089/ten.tea.2008.0067. [PubMed: 19193129]

[34]. Fisher MB, Belkin NS, Milby AH, Henning EA, Söegaard N, Kim M, Pfeifer C, Saxena V, Dodge GR, Burdick JA, Schaer TP, Steinberg DR, Mauck RL, Effects of Mesenchymal Stem Cell and Growth Factor Delivery on Cartilage Repair in a Mini-Pig Model, Cartilage 7 (2016) 174–184. doi:10.1177/1947603515623030. [PubMed: 27047640]

[35]. Purcell BP, Elser JA, Mu A, Margulies KB, Burdick JA, Synergistic effects of SDF-1α chemokine and hyaluronic acid release from degradable hydrogels on directing bone marrow derived cell homing to the myocardium., Biomaterials 33 (2012) 7849–57. doi:10.1016/j.biomaterials.2012.07.005. [PubMed: 22835643]

[36]. ‡ Jaso1. Burdick Jason A., †,‡, Chung Cindy, †, Jia Xinqiao, †, Randolph Mark A., ‡ and & Langer Robert*, †. Controlled Degradation and Mechanical Behavior of Photopolymerized Hyaluronic Acid Networks. (2004). doi:10.1021/BM049508An A. Burdick, †, † Cindy Chung, † Xinqiao Jia, ‡ and Mark A. Randolph, † Robert Langer*, Controlled Degradation and Mechanical Behavior of Photopolymerized Hyaluronic Acid Networks, (2004). doi:10.1021/BM049508A.

[37]. Burdick JA, Prestwich GD, Hyaluronic Acid Hydrogels for Biomedical Applications, Adv. Mater 23 (2011) H41–H56. doi:10.1002/adma.201003963. [PubMed: 21394792]

[38]. Baker BM, Nerurkar NL, Burdick JA, Elliott DM, Mauck RL, Fabrication and Modeling of Dynamic Multipolymer Nanofibrous Scaffolds, J. Biomech. Eng 131 (2009) 101012. doi:10.1115/1.3192140. [PubMed: 19831482]

[39]. M.C. et al.. Rueden CT; Schindelin J & Hiner, ImageJ2: ImageJ for the next generation of scientific image data, (2017). doi:10.1186/s12859-017-1934-z.

[40]. Ansorge HL, Meng X, Zhang G, Veit G, Sun M, Klement JF, Beason DP, Soslowsky LJ, Koch M, Birk DE, Type XIV collagen regulates fibrillogenesis: Premature collagen fibril growth and tissue dysfunction in null mice, J. Biol. Chem 284 (2009) 8427–8438. doi:10.1074/jbc.M805582200. [PubMed: 19136672]

[41]. Cesaretti M, Luppi E, Maccari F, Volpi N, A 96-well assay for uronic acid carbazole reaction, Carbohydr. Polym 54 (2003) 59–61. doi:10.1016/S0144-8617(03)00144-9.

[42]. Qu F, Lin J-MG, Esterhai JL, Fisher MB, Mauck RL, Biomaterial-mediated delivery of degradative enzymes to improve meniscus integration and repair, Acta Biomater 9 (2013) 6393–6402. doi:10.1016/j.actbio.2013.01.016. [PubMed: 23376132]

[43]. Nishitani K, Shirai T, Kobayashi M, Kuroki H, Azuma Y, Nakagawa Y, Nakamura T, Positive Effect of Alendronate on Subchondral Bone Healing and Subsequent Cartilage Repair in a Rabbit Osteochondral Defect Model, Am. J. Sports Med 37 (2009) 139–147. doi:10.1177/0363546509350984.

[44]. Muehleman C, Li J, Abe Y, Pfister B, Sah RL, Phipps R, Masuda K, Effect of risedronate in a minipig cartilage defect model with allograft, J. Orthop. Res 27 (2009) 360–365. doi:10.1002/jor.20775. [PubMed: 18925648]

[45]. Ashley B, Sennett M, Patel J, Martin A, Carey J, Mauck R, Dodge G, Bisphosphonate Treatment Reduces Subchondral Bone Remodeling in Chondral Defects in a Large Animal Model, in: Orthop. Res. Soc. Conf., New Orleans, 2018.

[46]. Madry H, Dodge GR, Friedman JM, Bonadio MB, Sennett ML, Mauck RL, A retinaculum-sparing surgical approach preserves porcine stifle joint cartilage in an experimental animal model of cartilage repair, J. Exp. Orthop 4 (2017). doi:10.1186/s40634-017-0083-7.

[47]. Pfeifer CG, Kinsella SD, Milby AH, Fisher MB, Belkin NS, Mauck RL, Carey JL, Development of a large animal model of osteochondritis dissecans of the knee: A pilot study, Orthop. J. Sport. Med 3 (2015) 1–10. doi:10.1177/2325967115570019.

[48]. Smith GD, Taylor J, Almqvist KF, Erggelet C, Knutsen G, Portabella MG, Smith T, Richardson JB, Arthroscopic Assessment of Cartilage Repair: A Validation Study of 2 Scoring Systems, Arthrosc. J. Arthrosc. Relat. Surg 21 (2005) 1462–1467. doi:10.1016/j.arthro.2005.09.007.

[49]. Stoeckl BD, Mauck RL, Dodge GR, Fisher MB, Meloni GR, Biphasic Finite Element Modeling Reconciles Mechanical Properties of Tissue-Engineered Cartilage Constructs Across Testing Platforms, Tissue Eng. Part A 23 (2017) 663–674. doi:10.1089/ten.tea.2016.0191. [PubMed: 28414616]

[50]. Yushkevich PA, Piven J, Hazlett HC, Smith RG, Ho S, Gee JC, Gerig G, User-guided 3D active contour segmentation of anatomical structures: Significantly improved efficiency and reliability, Neuroimage 31 (2006) 1116–1128. doi:10.1016/j.neuroimage.2006.01.015. [PubMed: 16545965]

[51]. Mainil-Varlet P, Van Damme B, Nesic D, Knutsen G, Kandel R, || Md, Roberts S, A New Histology Scoring System for the Assessment of the Quality of Human Cartilage Repair: ICRS II, (n.d.) doi:10.1177/0363546509359068.

[52]. Chim H, Miller E, Gliniak C, Alsberg E, Stromal-cell-derived factor (SDF) 1-alpha in combination with BMP-2 and TGF-β1 induces site-directed cell homing and osteogenic and chondrogenic differentiation for tissue engineering without the requirement for cell seeding, Cell Tissue Res 350 (2012) 89–94. doi:10.1007/s00441-012-1449-x. [PubMed: 22684849]

[53]. Kim M, Erickson IE, Choudhury M, Pleshko N, Mauck RL, Transient exposure to TGF-β3 improves the functional chondrogenesis of MSC-laden hyaluronic acid hydrogels, J. Mech. Behav. Biomed. Mater 11 (2012) 92–101. doi:10.1016/j.jmbbm.2012.03.006. [PubMed: 22658158]

[54]. Niloy KK, Gulfam M, Compton KB, Li D, Huang GT-J, Lowe TL, Methacrylated Hyaluronic Acid–Based Hydrogels Maintain Stemness in Human Dental Pulp Stem Cells, Regen. Eng. Transl. Med (2019) 1–11. doi:10.1007/s40883-019-00115-4. [PubMed: 30976657]

[55]. Bencherif SA, Srinivasan A, Horkay F, Hollinger JO, Matyjaszewski K, Washburn NR, Influence of the degree of methacrylation on hyaluronic acid hydrogels properties, Biomaterials 29 (2008) 1739–1749. doi:10.1016/j.biomaterials.2007.11.047. [PubMed: 18234331]

[56]. Ifkovits JL, Sundararaghavan HG, Burdick JA, Electrospinning fibrous polymer scaffolds for tissue engineering and cell culture, J. Vis. Exp 32 (2009) 1589. doi:10.3791/1589.

[57]. Zhao W, Liu W, Li J, Lin X, Wang Y, Preparation of animal polysaccharides nanofibers by electrospinning and their potential biomedical applications, J. Biomed. Mater. Res. - Part A 103 (2015) 807–818. doi:10.1002/jbm.a.35187.

[58]. Morikawa M, Derynck R, Miyazono K, TGF-β and the TGF-β Family: Context-Dependent Roles in Cell and Tissue Physiology., Cold Spring Harb. Perspect. Biol 8 (2016) a021873. doi:10.1101/cshperspect.a021873. [PubMed: 27141051]

[59]. Thieme S, Ryser M, Gentsch M, Navratiel K, Brenner S, Stiehler M, Rölfing J, Gelinsky M, Rösen-Wolff A, Stromal cell-derived factor-1alpha-directed chemoattraction of transiently CXCR4-overexpressing bone marrow stromal cells into functionalized three-dimensional biomimetic scaffolds., Tissue Eng. Part C. Methods 15 (2009) 687–96. doi:10.1089/ten.TEC.2008.0556. [PubMed: 19260802]

[60]. Honczarenko M, Le Y, Swierkowski M, Ghiran I, Glodek AM, Silberstein LE, Human Bone Marrow Stromal Cells Express a Distinct Set of Biologically Functional Chemokine Receptors, Stem Cells 24 (2006) 1030–1041. doi:10.1634/stemcells.2005-0319. [PubMed: 16253981]

[61]. Chu CR, Szczodry M, Bruno S, Animal Models for Cartilage Regeneration and Repair, Tissue Eng. Part B Rev 16 (2009) 105–115. doi:10.1089/ten.teb.2009.0452.

[62]. Vacanti CA, Langer R, Schloo B, Vacanti JP, Synthetic polymers seeded with chondrocytes provide a template for new cartilage formation., Plast. Reconstr. Surg 88 (1991) 753–9. http://www.ncbi.nlm.nih.gov/pubmed/1924560 (accessed March 10, 2019). [PubMed: 1924560]

[63]. Majumdar MK, Askew R, Schelling S, Stedman N, Blanchet T, Hopkins B, Morris EA, Glasson SS, Double-knockout of ADAMTS-4 and ADAMTS-5 in mice results in physiologically normal

animals and prevents the progression of osteoarthritis, Arthritis Rheum 56 (2007) 3670–3674. doi:10.1002/art.23027. [PubMed: 17968948]

[64]. Frisbie DD, Cross MW, McIlwraith CW, A comparative study of articular cartilage thickness in the stifle of animal species used in human pre-clinical studies compared to articular cartilage thickness in the human knee., Vet. Comp. Orthop. Traumatol 19 (2006) 142–6. http://www.ncbi.nlm.nih.gov/pubmed/16971996 (accessed March 9, 2019). [PubMed: 16971996]

[65]. Nixon AJ, Fortier LA, Goodrich LR, Ducharme NG, Arthroscopic reattachment of osteochondritis dissecans lesions using resorbable polydioxanone pins., Equine Vet. J 36 (2004) 376–83. http://www.ncbi.nlm.nih.gov/pubmed/15253076 (accessed March 9, 2019). [PubMed: 15253076]

[66]. Murray RC, Vedi S, Birch HL, Lakhani KH, Goodship AE, Subchondral bone thickness, hardness and remodelling are influenced by short-term exercise in a site-specific manner, J. Orthop. Res 19 (2001) 1035–1042. doi:10.1016/S0736-0266(01)00027-4. [PubMed: 11781002]

[67]. Marshall M, Lydtin H, Krawietz W, Hagen R, Schuckert G, Hess H, Zöllner N, Das Miniaturschwein als Versuchstier in der experimentellen Medizin, Res. Exp. Med 157 (1972) 300–316. doi:10.1007/BF01852074.

[68]. Gotterbarm T, Breusch SJ, Schneider U, Jung M, The minipig model for experimental chondral and osteochondral defect repair in tissue engineering: Retrospective analysis of 180 defects, Lab. Anim 42 (2008) 71–82. doi:10.1258/la.2007.06029e. [PubMed: 18348768]

[69]. Ahern BJ, Parvizi J, Boston R, Schaer TP, Preclinical animal models in single site cartilage defect testing: a systematic review, Osteoarthr. Cartil 17 (2009) 705–713. doi:10.1016/j.joca.2008.11.008.

[70]. Mainil-Varlet P, Rieser F, Grogan S, Mueller W, Saager C, Jakob RP, Articular cartilage repair using a tissue-engineered cartilage-like implant: an animal study., Osteoarthr. Cartil 9 Suppl A (2001) S6–15. http://www.ncbi.nlm.nih.gov/pubmed/11680690 (accessed March 9, 2019).

[71]. Borsøe Christensen B, Bindzus Foldager C, Lykke Olesen M, Vingtoft L, Hendrik Duedal Rölfing J, Ringgaard S, Lind M, Experimental articular cartilage repair in the Göttingen minipig: the influence of multiple defects per knee, (2011). doi:10.1186/s40634-015-0031-3.

[72]. Peterson L, Pulliainen O, Hyttinen MM, Lindahl A, Jurvelin JS, Helminen HJ, Kiviranta I, Vasara AI, Lammi MJ, Immature porcine knee cartilage lesions show good healing with or without autologous chondrocyte transplantation, Osteoarthr. Cartil 14 (2006) 1066–1074. doi:10.1016/j.joca.2006.04.003.

[73]. Pfeifer CG, Kim M, Steinberg DA, Mauck RL, Saxena V, Fisher MB, Dodge GR, Henning EA, Age-Dependent Subchondral Bone Remodeling and Cartilage Repair in a Minipig Defect Model, Tissue Eng. Part C Methods 23 (2017) 745–753. doi:10.1089/ten.tec.2017.0109. [PubMed: 28747146]

[74]. Pfeifer CG, Fisher MB, Saxena V, Kim M, Henning EA, Steinberg DA, Dodge GR, Mauck RL, Age-Dependent Subchondral Bone Remodeling and Cartilage Repair in a Minipig Defect Model, Tissue Eng. Part C Methods (2017) ten.tec.2017.0109. doi:10.1089/ten.tec.2017.0109.

[75]. Fisher JE, Rogers MJ, Halasy JM, Luckman SP, Hughes DE, Masarachia PJ, Wesolowski G, Russell RG, Rodan GA, Reszka AA, Alendronate mechanism of action: geranylgeraniol, an intermediate in the mevalonate pathway, prevents inhibition of osteoclast formation, bone resorption, and kinase activation in vitro., Proc. Natl. Acad. Sci. U. S. A 96 (1999) 133–8. doi:10.1073/PNAS.96.1.133. [PubMed: 9874784]

[76]. Pazianas M, Abrahamsen B, Ferrari S, Russell RGG, Eliminating the need for fasting with oral administration of bisphosphonates, Ther. Clin. Risk Manag 9 (2013) 395–402. doi:10.2147/TCRM.S52291. [PubMed: 24204155]

[77]. Walenkamp AME, Lapa C, Herrmann K, Wester H-J, CXCR4 Ligands: The Next Big Hit?, J. Nucl. Med 58 (2017) 77S–82S. doi:10.2967/jnumed.116.186874. [PubMed: 28864616]

[78]. Lee C, Liu Q-H, Tomkowicz B, Yi Y, Freedman BD, Collman RG, Macrophage activation through CCR5- and CXCR4-mediated gp120-elicited signaling pathways, J. Leukoc. Biol 74 (2003) 676–682. doi:10.1189/jlb.0503206. [PubMed: 12960231]

[79]. Huang L, Yi L, Zhang C, He Y, Zhou L, Liu Y, Qian L, Hou S, Weng T, Synergistic Effects of FGF-18 and TGF-β3 on the Chondrogenesis of Human Adipose-Derived Mesenchymal Stem Cells in the Pellet Culture, (2018). doi:10.1155/2018/7139485.

[80]. Qu F, Pintauro MP, Haughan JE, Henning EA, Esterhai JL, Schaer TP, Mauck RL, Fisher MB, Repair of dense connective tissues via biomaterial-mediated matrix reprogramming of the wound interface, Biomaterials 39 (2015) 85–94. doi:10.1016/j.biomaterials.2014.10.067. [PubMed: 25477175]

[81]. Mohanraj B, Duan G, Peredo A, Kim M, Tu F, Lee D, Dodge GR, Mauck RL, Mechanically Activated Microcapsules for “On-Demand” Drug Delivery in Dynamically Loaded Musculoskeletal Tissues, Adv. Funct. Mater 29 (2019) 1807909. doi:10.1002/adfm.201807909. [PubMed: 32655335]

Statement of Significance

This study addresses an area of orthopaedic medicine in which treatment options are limited and new biomaterials stand to improve patient outcomes. Those suffering from articular cartilage injuries are often destined to have early onset osteoarthritis. We have created a cell-free nanofibrous hyaluronic acid (HA) scaffold that delivers factors specifically designed to enhance cartilage repair: Stromal Cell-Derived Factor-1α (SDF-1α; SDF) to increase the recruitment and infiltration of mesenchymal stem cells (MSCs) and Transforming Growth Factor-β3 (TGF-β3; TGF) to enhance cartilage tissue formation. To our knowledge, this study is the first to evaluate such a bioactive scaffold in a large animal model and demonstrates the capacity for dual growth factor release

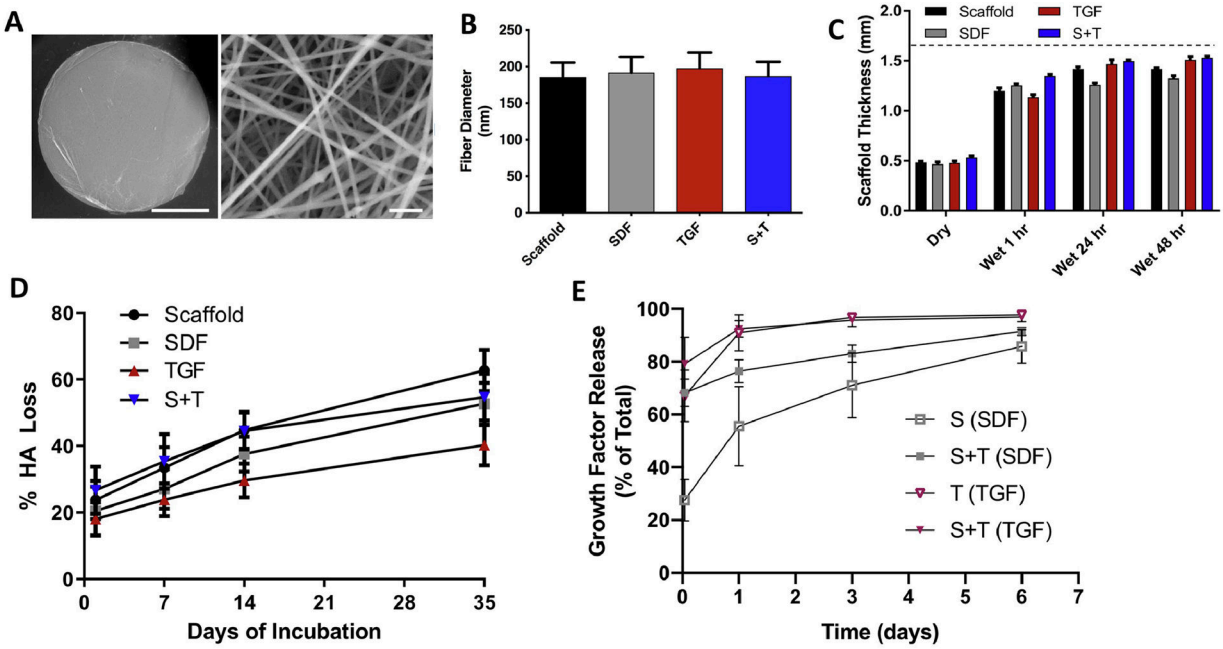

Figure 1 –. Scaffold Characterization.

(A) Visualization of fibers (SDF group) and (B) measurement of scaffold fiber diameter via scanning electron microscopy (scale bar = 1 mm or 1 μm, n=10). (C) Scaffold thickness in the dry and hydrated states (1, 24, 48 hours). Dashed line represents average porcine trochlear cartilage thickness (n=4). (D) %HA release as a function of time of incubation (n=8). (E) SDF-1α and TGF-β3 release from scaffolds quantified by ELISA (n=3). Error bars = SEM. * denotes a significant difference ($p < 0.05$) between groups at a specific time point.

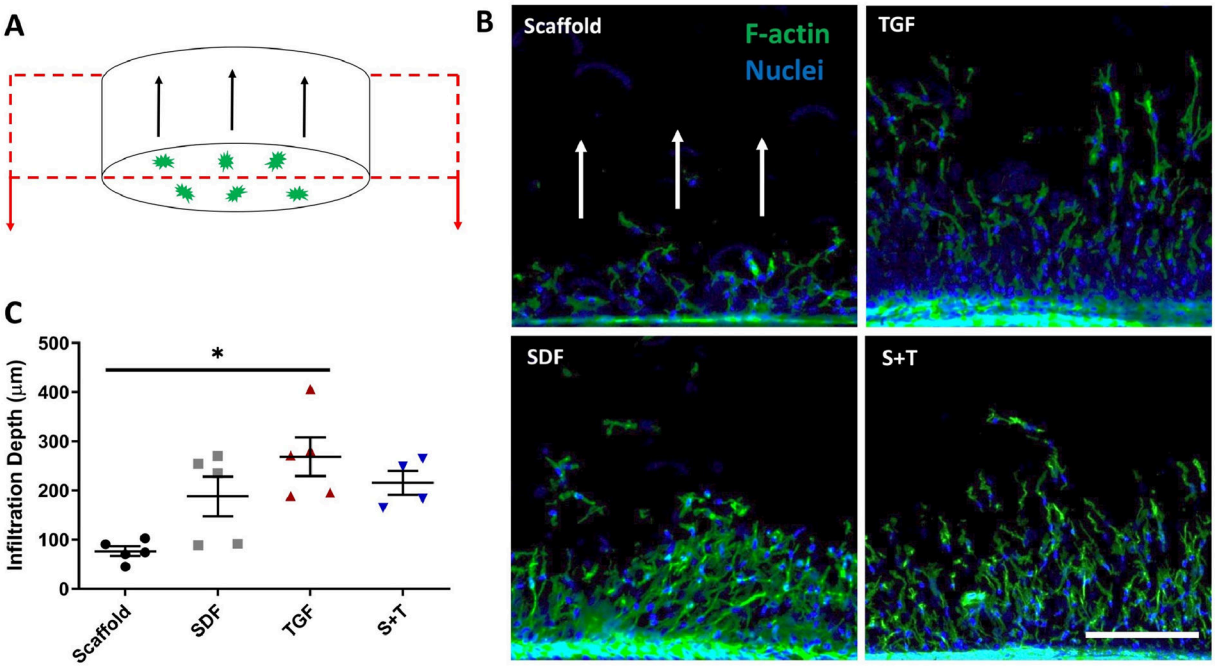

Figure 2 –. MSC Infiltration into Scaffolds.

(A) Diagram showing MSCs (green) seeded and migrating into a cylindrical scaffold (depicted by black arrows), cut in cross-section for imaging. (B) Visualization (white arrows depict direction of migration) and (C) quantification of cell infiltration via confocal microscopy with Hoechst staining of nuclei (blue) and Phalloidin staining of actin (green) (n=5); error bars = SEM, scale bar = 200μm. * denotes $p < 0.05$.

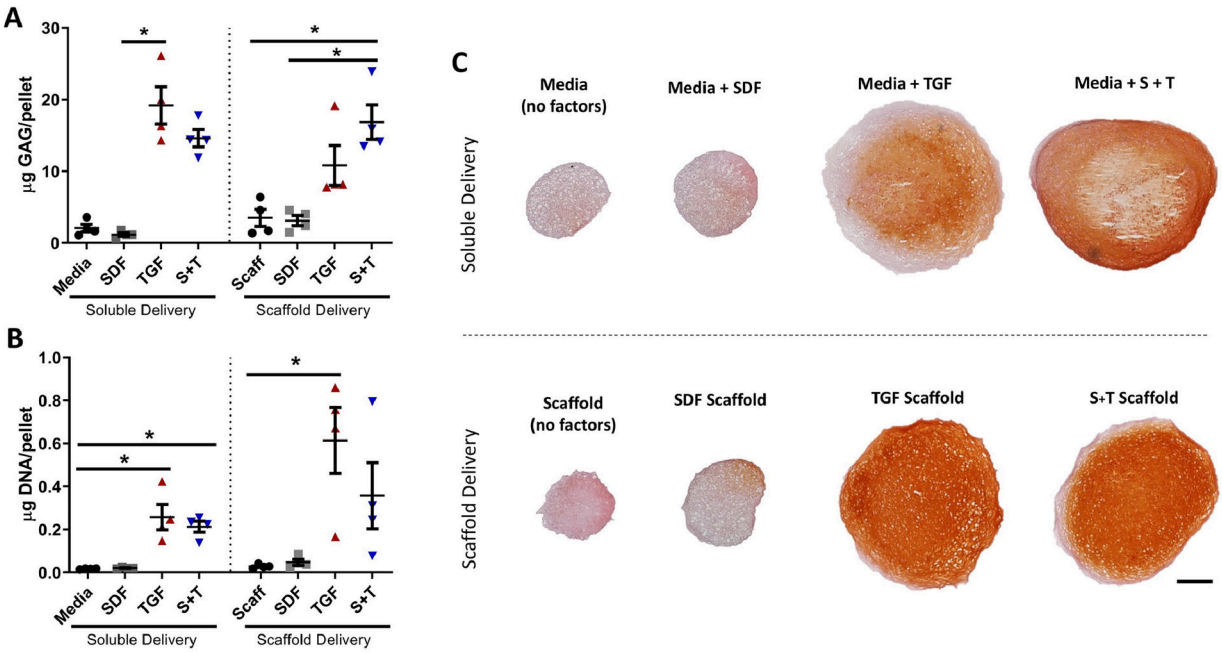

Figure 3 –. *In Vitro* Chondrogenic Activity.

(A) GAG content measured via the DMMB assay (n=4) and (B) DNA content measured via the PicoGreen assay (n=4), error bars = SEM. * indicates $p < 0.05$. (C) Safranin O and Fast Green staining of representative sections (n=4); scale bar = 200μm.

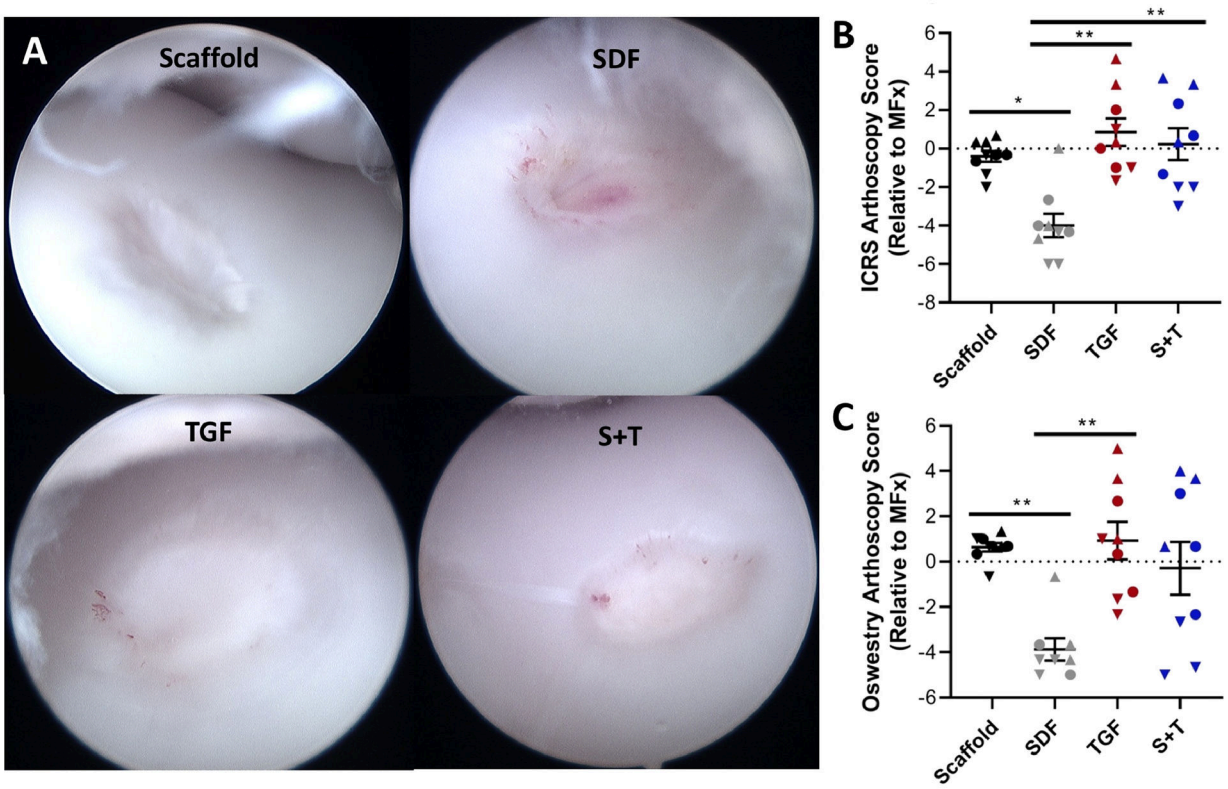

Figure 4 –. Arthroscopic observations at 12 weeks post-op.

(A) Representative arthroscopic images showing defects treated with Scaffold, SDF, TGF, and S+T groups within different joints. (B) ICRS and (C) Oswestry scoring showing similar outcomes (n=9). Normalized data show each animal within a given group as a specific shape: best animal = up triangle, median animal = circle, worst animal = down triangle. Error bars = SEM. * and ** represent $p < 0.05$ and $p < 0.01$, respectively.

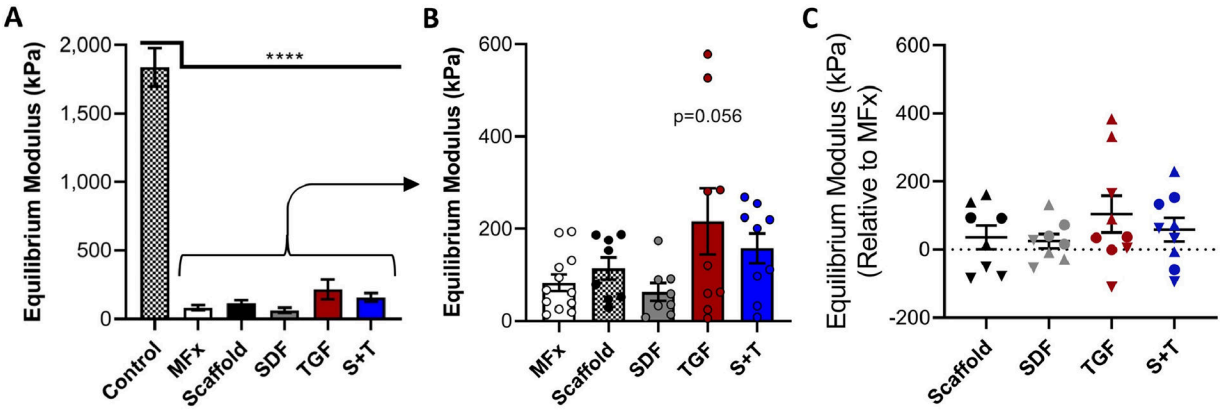

Figure 5 –. Indentation testing.

(A) Equilibrium modulus of adjacent control cartilage (n=12) and (B) defects treated with MFx or Scaffold (n=9–12/group). (C) Equilibrium modulus of scaffold-treated defects relative to that of MFx-treated defect in same knee (n=9). Normalized data show each animal as a given shape: best = up triangle, median = circle, worst = down triangle. Error bars = SEM.

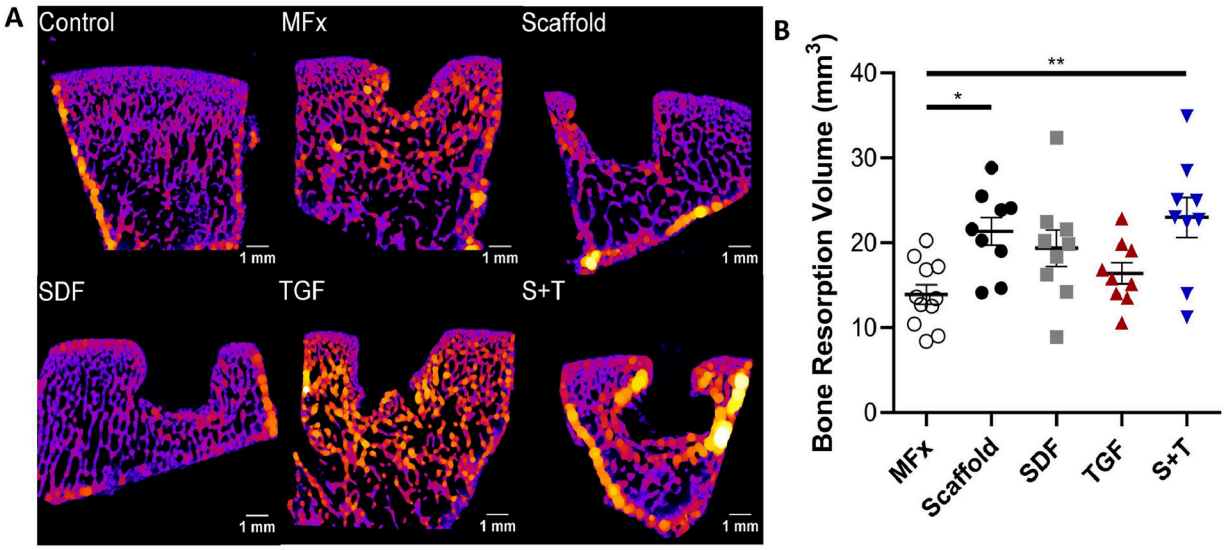

Figure 6 - μCT analysis of subchondral bone at the repair site.

(A) Trabecular thickness heat map of defect cross-section. (B) Volume of bone resorption (n=9). Error bars = SEM. * and ** represent $p < 0.05$ and $p < 0.01$, respectively.

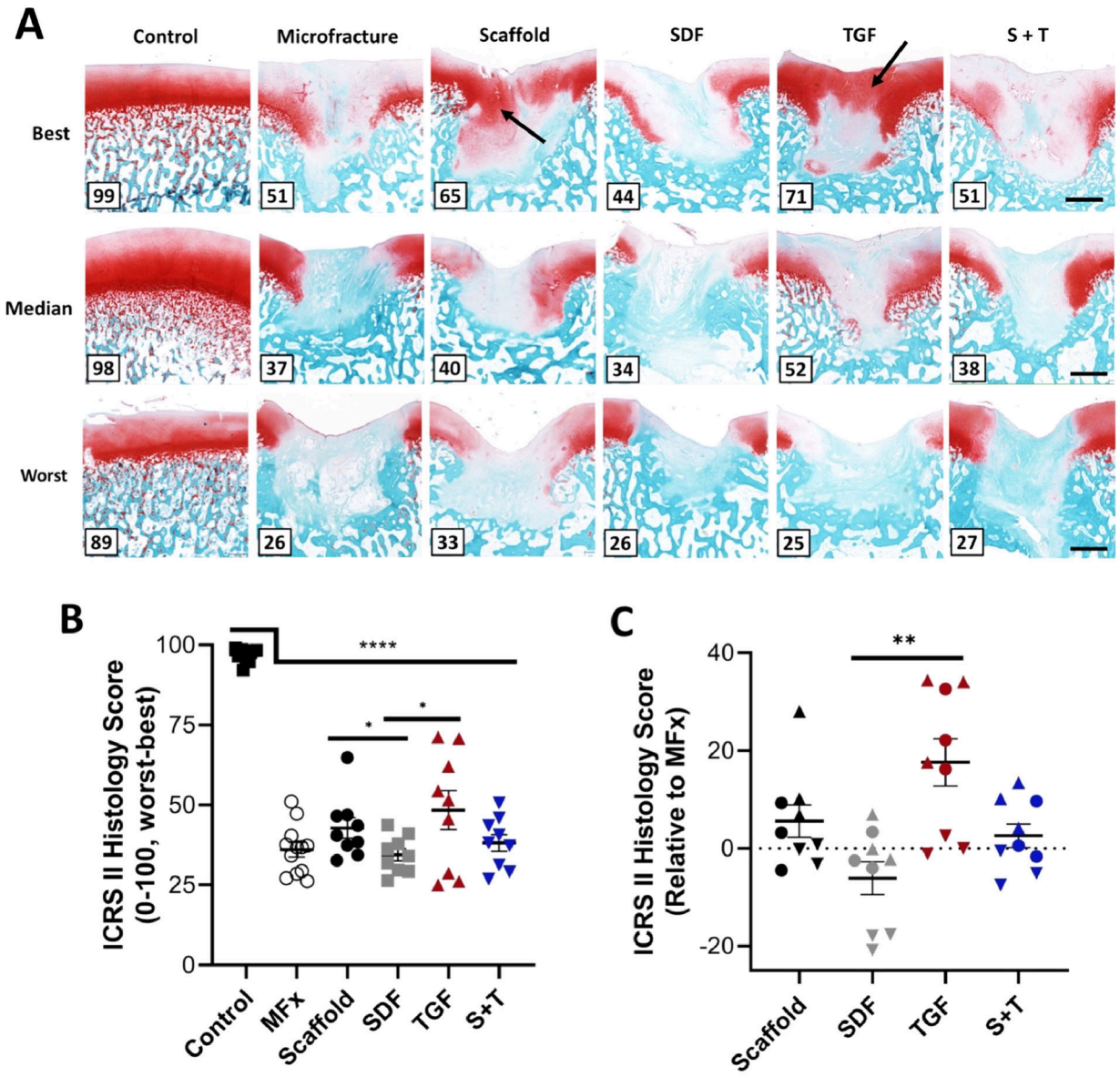

Figure 7 –. Histological evaluation of cartilage repair.

(A) Best, median, and worst defects from each group stained in Safranin O and Fast Green; number in bottom left corner represents score; black arrows indicate regions of higher proteoglycan deposition (red stain); scale bar = 1mm. (B) Raw ICRS II Histology scores on 0–100 (worst-best) scale (n=9–12/group) and (C) scores relative to MFx within the same joint (n=9). Normalized data show each animal within a given group as a specific shape: best = up triangle, median = circle, worst = down triangle. Error bars = SEM. ** and **** represent $p < 0.01$ and $p < 0.0001$, respectively.

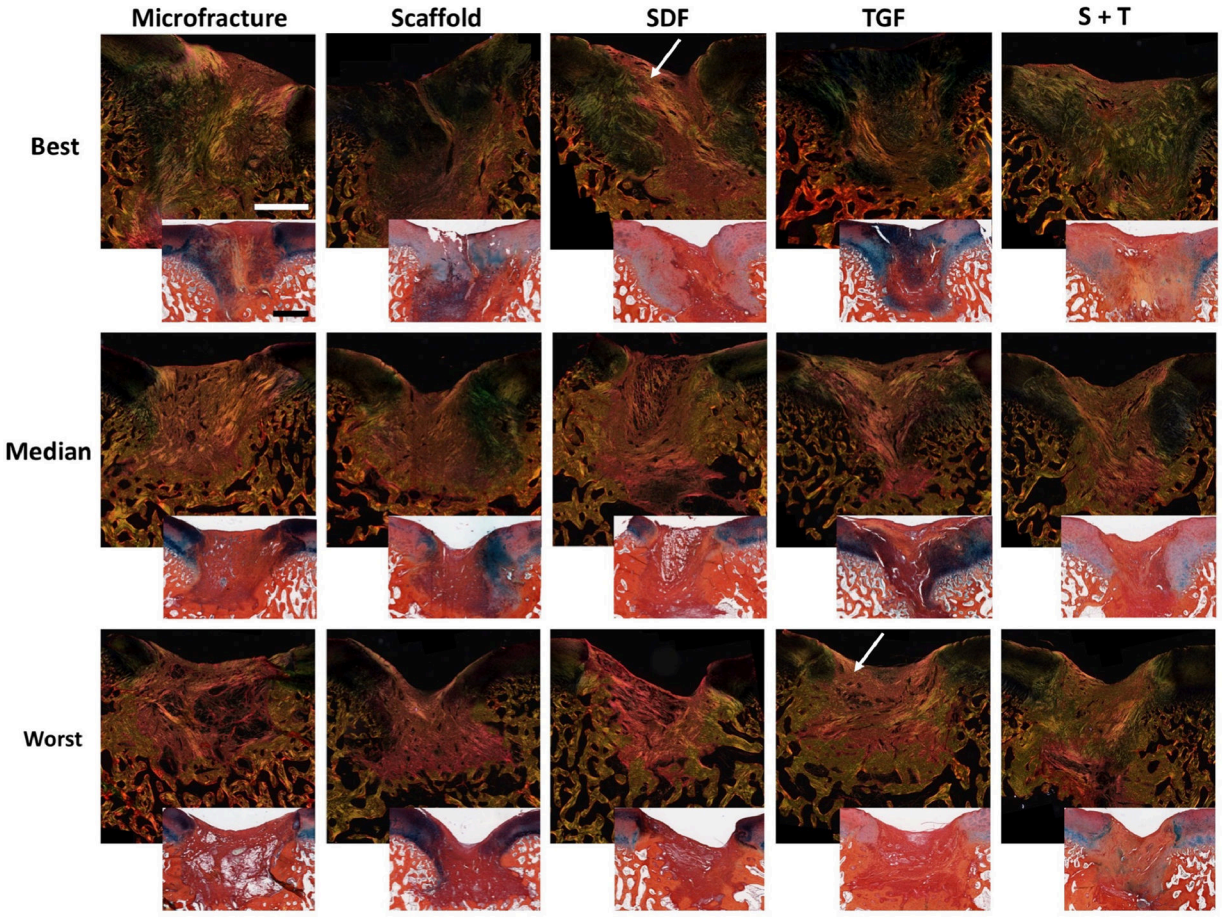

Figure 8 –. Polarized and light (inset) microscopy of sections stained with Alcian Blue and Picrosirius Red.

Best, median, and worst samples. White arrows depict areas with increased fibrous tissue deposition. Scale bar = 1mm.

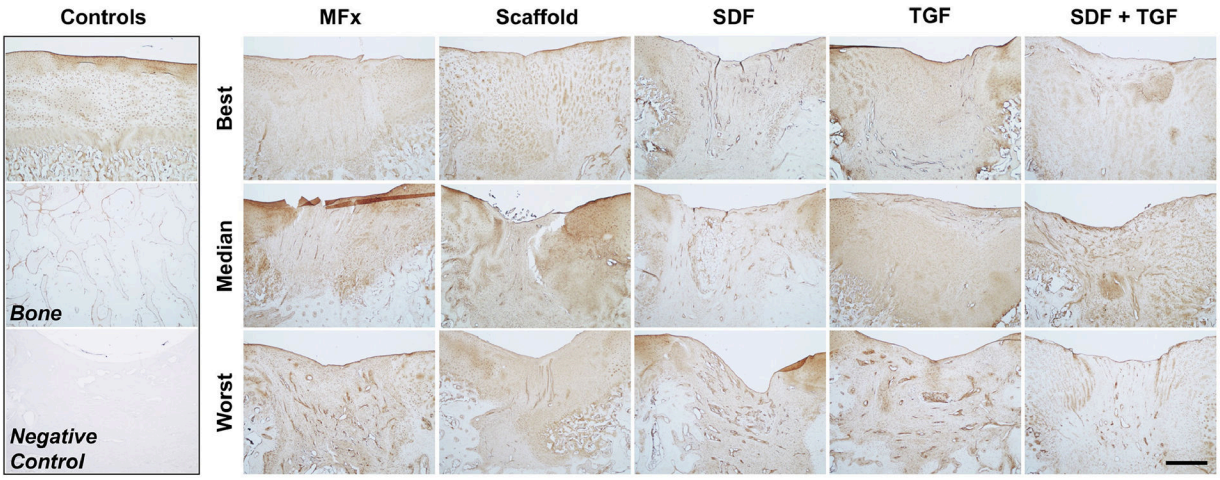

Figure 9 –. Immunohistochemical Staining for Type II Collagen.

Best, median, and worst-scoring defects from each group are shown. Control samples of healthy stained cartilage and bone are shown for comparison (top left). Negative control stain of repair tissue is also shown for comparison (bottom left). Scale bar = 1mm.

Table 1 –

Scaffold locations and distributions across animals.

	Right Trochlea					Laft Trochlea			
Pig	**Proximal Lateral**	**Distal Lateral**	**Proximal Medial**	**Distal Medial**		**Proximal Medial**	**Distal Medial**	**Proximal Lateral**	**Distal Lateral**
1	MFx	SCAFFOLD	SCAFFOLD	SCAFFOLD		MFx	SDF	SDF	SDF
2	TGF	MFx	TGF	TGF		S+T	MFx	S+T	S+T
3	SCAFFOLD	SCAFFOLD	MFx	SCAFFOLD		TGF	TGF	MFx	TGF
4	MFx	SDF	SDF	SDF		MFx	S+T	S+T	S+T
5	SCAFFOLD	SCAFFOLD	SCAFFOLD	MFx		S+T	S+T	S+T	MFx
6	TGF	TGF	TGF	MFx		SDF	SDF	SDF	MFx

MFx = Microfracture only, Scaffold = no growth factor, SDF = SDF-1α only, TGF = TGF-β3 only, S+T = SDF-1α and TGF-β3